EPR and optical study of Yb^{3+}-doped β-PbF_2 single crystals and nanocrystals of glass-ceramics

2006 J. Phys.: Condens. Matter 18 7905

(http://iopscience.iop.org/0953-8984/18/34/005)

INSTITUTE OF PHYSICS PUBLISHING JOURNAL OF PHYSICS: CONDENSED MATTER

J. Phys.: Condens. Matter **18** (2006) 7905–7922 doi:10.1088/0953-8984/18/34/005

EPR and optical study of Yb^{3+}-doped β-PbF_2 single crystals and nanocrystals of glass-ceramics

G Dantelle, M Mortier[1], Ph Goldner and D Vivien

Laboratoire de Chimie de la Matière Condensée de Paris, CNRS-UMR 7574, ENSCP-11, rue Curie-75005 Paris, France

E-mail: michel-mortier@enscp.fr

Received 24 May 2006, in final form 13 July 2006
Published 7 August 2006
Online at stacks.iop.org/JPhysCM/18/7905

Abstract

β-PbF_2 single crystals doped with YbF_3 (0.2% and 2%) were studied by x-ray diffraction (XRD), electron paramagnetic resonance (EPR) and optical spectroscopy. EPR revealed the presence of only one kind of paramagnetic ion Yb^{3+}, in a cubic symmetry site. The optical absorption, emission and excitation spectra enabled us to identify the transitions attributed to Yb^{3+} in the cubic site and to determine its energy level diagram. Site-selective laser spectroscopy also evidenced the presence of another type of Yb^{3+} ions, undetectable by classical EPR. This second type, which dominates in the 2%-doped crystal and exhibits cooperative luminescence, was attributed to Yb^{3+} ions forming clusters.

Transparent oxyfluoride glass-ceramics, containing β-$Pb_{1-y}Yb_yF_{2+y}$ nanocrystallites, were also synthesized and studied by XRD, EPR and optical spectroscopy. Two types of Yb^{3+} ions were found, as in β-PbF_2 single crystals. The optical properties of the oxyfluoride glass-ceramics turn out to be similar to those of ytterbium activated β-PbF_2 single crystals. Moreover, the Yb environments found in PbF_2 single crystals seem to already occur in the parent glass. Therefore, these materials are expected to be good laser media, like the rare-earth doped fluorite crystals, either in bulk or fibre form.

1. Introduction

At the beginning of the 1970s, β-PbF_2 bulk single crystals were of great interest because of their high-temperature superionic properties and consequently their possible applications in electrochemical devices [1]. More recently, trivalent rare-earth (RE) doped β-PbF_2 bulk single crystals have been studied for their optical properties [2].

Transparent glass-ceramics doped with trivalent rare earths have been widely studied as an alternative to bulk single crystals and glasses for optical applications [3, 4]. We are studying

[1] Author to whom any correspondence should be addressed.

Table 1. g-factors of Yb^{3+}-doped fluorite-type single crystals.

Site symmetry	CaF_2:Yb [13]	SrF_2:Yb [14]	BaF_2:Yb [14]	CdF_2:Yb [15]
Cubic (O_h)	$g_{cub} = 3.443$	$g_{cub} = 3.441$	$g_{cub} = 3.422$	$g_{cub} = 3.443$
Tetragonal (C_{4v})	$g_{\parallel} = 2.412$ $g_{\perp} = 3.802$	—	—	—
Trigonal (C_{3v})	$g_{\parallel} = 1.421$ $g_{\perp} = 4.389$	$g_{\parallel} = 2.811$ $g_{\perp} = 3.743$	$g_{\parallel} = 2.763$ $g_{\perp} = 3.768$	—

here GeO_2–PbO–PbF_2 transparent glass-ceramics doped with YbF_3. The first step in the glass-ceramic synthesis is the formation of a glass. Then, the glass is annealed to obtain the crystallization of the fluoride phase, β-PbF_2 [5], whose particle size is controlled by the temperature and duration of the heat-treatment. The obtained glass-ceramics are composed of an amorphous oxide matrix and fluoride nanocrystallites embedded into it. To keep the material transparency, nanosized crystallites are required, usually smaller than 40 nm. Glass-ceramics are much easier to synthesize and shape than single crystals, allowing the formation of big-sized samples and fibres [6]. Combining the good properties of glasses and crystals, glass-ceramics appear promising for future optical applications.

PbF_2 crystallizes in two different phases: an orthorhombic phase α, which is obtained by soft chemistry synthesis [7] and a cubic phase β, crystallizing in the space group $Fm3m$ with the fluorite structure. The incorporation of trivalent rare-earth ions in fluorite-type crystals MF_2 (M = Ca, Sr, Ba, Cd or Pb) induces the substitution of the divalent cation M^{2+} by a trivalent RE ion. To compensate the excess of positive charge, several processes can be proposed, such as the creation of cation vacancies, following the equation $3Pb^{2+} \equiv 2Er^{3+} + Pb$ vacancy [8], or the presence of an interstitial fluoride anion F^-. The second mechanism is more likely, since interstitial F^- ions in rare-earth doped fluorite-type crystals have been experimentally observed using x-ray and neutron investigations [9, 10]. Furthermore, these interstitial F^- ions are responsible for the increase of the anionic conductivity in Ln^{3+}-doped β-PbF_2 single crystals [11, 12]. Several cases are possible, according to the position of the interstitial F^-:

- First, the interstitial fluoride is situated in another unit cell than the one containing the RE ion, preserving the cubic local symmetry (O_h) of the RE.
- Second, the interstitial fluoride is situated in the same unit cell as the RE, inducing a distortion from the cubic symmetry. Hence, the RE ion symmetry centres are either tetragonal (C_{4v}) if the interstitial F^- is situated in the ⟨100⟩ direction, or trigonal (C_{3v}) if it is situated in the ⟨111⟩ direction.

In the literature, Yb^{3+} in cubic symmetry (O_h) was detected by EPR in CaF_2 [13], SrF_2 [14], BaF_2 [14] and CdF_2 [15] single crystals. In CaF_2, SrF_2 and BaF_2, Yb^{3+} was also found in tetragonal (C_{4v}) and/or trigonal (C_{3v}) symmetry sites. The g-factors associated with these symmetries are gathered in table 1. Optical studies of these compounds were performed [13, 14], allowing the attribution of some optical transitions to Yb^{3+} ions in different sites with cubic or non-cubic symmetries. Nonetheless, the correlation between the EPR and optical results is not always obvious [15]. In β-PbF_2 bulk single crystals doped with YbF_3, EPR only evidences Yb^{3+} in cubic symmetry, with a g-factor of 3.434 [16]. Nonetheless, the optical spectra exhibit more bands than expected for only one occupied site [15, 16].

In this paper, in respect to previous works on Ln^{3+}-doped β-PbF_2 single crystals [16] or other fluorite-type compounds [13] or glass-ceramics [17], two types of sites will be clearly identified: cubic Yb^{3+} and clusters of Yb^{3+}. The respective amounts of these two types of

Yb^{3+} will be quantitatively determined as a function of the dopant concentration. This will be achieved using three complementary techniques, which are not usually used together: XRD, EPR and optical measurements, including site-selective laser spectroscopy. Another aim of this work will be to compare Yb^{3+}-doped bulk single crystals with nanocrystals doped with the same rare earth, dispersed throughout glass-ceramics.

2. Experimental section

2.1. β-PbF_2 single crystals

β-PbF_2 single crystals doped with $y YbF_3$ ($y = 0.2\%, 2\%$) were grown by a modified Bridgman technique, under argon atmosphere. PbF_2 and YbF_3 polycrystalline powders, placed into a carbon crucible, were melted at 1000 °C in a vertical furnace with a strong thermal gradient (20 °C cm^{-1}). The furnace was slowly cooled (cooling rate = 10 °C h^{-1}), allowing the displacement of the thermal gradient and consequently the displacement of the crystallization front [18]. Finally, 3 cm long single crystals were obtained. In the following, the two single crystals will be labelled $PbF_2 + 0.2\%$ Yb and $PbF_2 + 2\%$ Yb respectively. The crystals were oriented with x-rays by the Laue method and were cut along the (110) planes. Chemical analysis performed, after dissolution in perchloric/nitric acid solution, by atomic absorption spectroscopy indicates that the true doping rate of the crystals is respectively $0.22 \pm 0.05\%$ and $1.98 \pm 0.05\%$.

2.2. Oxyfluoride glass-ceramics

GeO_2 (purity 99.999%), PbO (99%), PbF_2 (99.997%) and YbF_3 (99.99%) were mixed together and heated in a platinum crucible at 1050 °C for 20 min in air. The mixture was poured between two copper plates, previously heated at 150 °C to limit thermal shocks, and transparent glasses were obtained. They were then annealed for 2 h at 300 °C to reduce the internal strains. The molar composition of glasses is:

- $50GeO_2$:40PbO:$10PbF_2 + 3YbF_3$, sample labelled P10Y3;
- $50GeO_2$:28PbO:$22PbF_2 + 0.05YbF_3$, sample labelled P22Y005.

Each glass was heated for 10 h at respectively 360 and 350 °C [19]. This devitrification process enables the crystallization of the fluoride phase only, leading to the synthesis of oxyfluoride glass-ceramics. The glass-ceramics will be hereafter labelled P10Y3GC and P22Y005GC.

X-ray diffraction diagrams were performed on a Philips PW1050/25 diffractometer with a Ni filter, using a Cu anode ($\lambda_{Cu} = 1.5406$ Å). The diffraction patterns were scanned over the 2θ range 24°–70° with a 0.02° step.

EPR spectra were performed with a Bruker ELEXSYS E500 spectrometer, at the X-band (frequency ∼9.39 GHz), equipped with a helium flow cryostat.

Absorption spectra were recorded at 10 K with a closed-cycle cryostat, using a Cary E5 spectrophotometer and well polished samples.

Emission spectra in the infrared and visible range were recorded at 10 K, under a CW excitation, using a titanium-sapphire laser (Coherent 890) pumped by an argon ion laser (Coherent Sabre). The fluorescence was analysed through a Jobin-Yvon HRD monochromator and detected with a liquid-nitrogen-cooled Ge cell for the infrared or a photon-counting photomultiplier for the visible emission.

The excitation spectra were measured at 10 K, using the tunability of the Ti:sapphire laser in the range 900–990 nm.

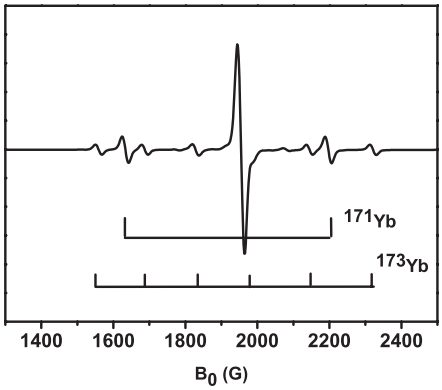

Figure 1. EPR spectra of β-PbF_2 single crystal doped with 0.2% YbF_3. $T = 10$ K, $\nu = 9.40$ GHz.

3. Investigation of the β-PbF_2 single crystals: results and discussion

3.1. X-ray diffraction

XRD diagrams of $PbF_2 + 0.2\%$ Yb and $PbF_2 + 2\%$ Yb single crystals confirm that the structural transformation $\beta \rightarrow \alpha$ does not occur at ambient pressure and that the crystals retain their high temperature structure upon cooling [20]. Bragg positions of the two single crystals are slightly shifted towards the high angles compared to those of pure β-PbF_2[2]. Using these angular positions, the unit cell parameter a was calculated: $a(\beta\text{-}PbF_2 + 0.2\%\ \text{Yb}) = 5.930 \pm 0.005$ Å and $a(\beta\text{-}PbF_2 + 2\%\ \text{Yb}) = 5.905 \pm 0.005$ Å, whereas the unit cell parameter of pure β-PbF_2 is 5.94 Å (see footnote 2). The decrease of the unit cell parameter in Yb^{3+}-doped single crystals evidenced the substitution of Pb^{2+} by Yb^{3+}. Indeed, despite the presence of an interstitial F^- for the charge compensation, the reduction of the ionic radius from Pb^{2+} (1.45 Å) to Yb^{3+} (1.12 Å) dominates and explains the decrease of the unit cell parameter [5, 21]. We have previously observed a similar behaviour in ErF_3-doped β-PbF_2 [18].

3.2. EPR study

Yb^{3+} ($4f^{13}$ electronic configuration) is a paramagnetic ion, with an effective spin $S = 1/2$. It has five even isotopes (^{168}Yb, ^{170}Yb, ^{172}Yb, ^{174}Yb and ^{176}Yb) with a nuclear spin I of zero and two odd isotopes (^{171}Yb and ^{173}Yb) with nuclear spin of respectively $I = 1/2$ and $I = 5/2$ and natural abundance of 14.3% and 16.1%.

An EPR signal was observed only below 50 K. Indeed, like most of the rare-earth ions, Yb^{3+} has a very short spin–lattice relaxation time T_1 at room temperature, which induces very broad absorption lines that cannot be detected by EPR. However, at low temperatures, T_1 strongly increases, reducing the absorption linewidth and allowing the observation of the EPR signal. The EPR spectrum of the $PbF_2 + 0.2\%$ Yb single crystal, presented in figure 1, is composed of an intense central line at $B_0 = 1954$ G (for $\nu = 9.40$ GHz), corresponding to the even isotopes of Yb^{3+}, and of several hyperfine satellites. Two sets of hyperfine satellites can be recognized, according to the nuclear spin of the ytterbium odd isotopes, as indicated in figure 1. From this figure, one can deduce $|A(^{171}\text{Yb})| = 901(\pm 1) \times 10^{-4}$ cm^{-1} and $|A(^{173}\text{Yb})| = 245(\pm 1) \times 10^{-4}$ cm^{-1}. The ratio of the hyperfine parameters $|\frac{A(^{171}\text{Yb})}{A(^{173}\text{Yb})}|$ corresponds to the ratio of the g_n factors $\frac{g_n(^{171}\text{Yb})}{g_n(^{173}\text{Yb})} = -3.63$. The ratio of the intensities H of

[2] JSPDS card No 77-1866 C.

Table 2. Wavelength of the absorption lines observed at 10 K in the $PbF_2 + 0.2\%$ Yb and $PbF_2 + 2\%$ Yb single crystals.

Absorption line	A_1	A_2	A_3	B_1	B_2	B_3
Wavelength (nm)	929	950.6	966.6	927	967	978[a]

[a] Composite band.

the hyperfine satellites of ^{171}Yb and ^{173}Yb $\frac{H(^{171}\text{Yb})}{H(^{173}\text{Yb})}$ is equal to 2.6, in good correlation with the theoretical value (2.625) calculated from the relative abundance of the two isotopes. This confirms the assignments given in figure 1, which are also in agreement with the previous measurements of Gerasimov *et al* [16] and of Sherstkov *et al* [22].

The rotation of the single crystals inside the cavity around the ⟨110⟩ direction leads to identical EPR spectra. The spectrum isotropy evidences that Yb^{3+} ions occupy cubic sites with O_h symmetry, i.e. the interstitial F^-, acting as a charge compensator, is situated at long distance. The isotropic g-factor value $g_{cub} = 3.435 \pm 0.005$ is very close to those reported in the literature [16, 22]. There are no significant additional lines that would reflect Yb^{3+} ions in lower symmetry sites, indicating that only Yb^{3+} ions in cubic symmetry are detected by EPR, in agreement with the literature [16, 22].

The EPR spectrum of the single crystal doped with 2% Yb was recorded in the same conditions. Its absorption lines are situated at the same field as those of the $PbF_2 + 0.2\%$ Yb single crystal, but are broader (peak-to-peak line-width of 34 G instead of 22 G). This evidences the presence of dipole–dipole interactions between paramagnetic ions in the more concentrated sample. Furthermore, the spectrum of the $PbF_2 + 0.2\%$ Yb single crystal can be fitted using Gaussian lines, whereas the spectrum of $PbF_2 + 2\%$ Yb must be fitted with Lorentzian lines. This is an indication that magnetic exchange interaction also occurs in the second crystal [23].

The double integration of EPR signals enables us to quantify the number of EPR-detected Yb^{3+} ions per unit of weight in the two crystals. According to the chemical analysis, the Yb^{3+} concentration ratio R, expressed as $R = \frac{[Yb^{3+}] \text{ in } (PbF_2+2\% \text{ } YbF_3)}{[Yb^{3+}] \text{ in } (PbF_2+0.2\% \text{ } YbF_3)}$, is $R \sim 10$, whereas the experimental integration of the EPR signals evidences $R = 3 \pm 1$. This difference indicates that, at least in $PbF_2 + 2\%$ Yb, some Yb^{3+} ions are not detected by EPR experiments.

To sum up, in both Yb^{3+}-doped β-PbF_2 single crystals, EPR spectroscopy highlights the presence of Yb^{3+} ions occupying only cubic symmetry sites, but the quantitative analysis of the EPR signals reveals that some Yb^{3+} ions are not detected by EPR, at least in the $PbF_2 + 2\%$ Yb single crystal.

3.3. Optical study of Yb-doped β-PbF₂ single crystals

3.3.1. Optical investigation of various types of Yb^{3+} in β-PbF_2. The absorption spectra of $PbF_2 + 0.2\%$ Yb and $PbF_2 + 2\%$ Yb single crystals were recorded at 10 K to depopulate the excited Stark levels of the $^2F_{7/2}$ multiplet and reduce the absorption linewidth for a better resolution. Both spectra are reported in figure 2. To facilitate the comparison between the two spectra, the $PbF_2 + 0.2\%$ Yb absorption coefficients (figure 2(a)) have been multiplied by a factor of ten. The labelling of the different lines observed is indicated in figure 2 and their peak wavelengths are gathered in table 2.

From the comparison of the two spectra given in figure 2, it is obvious that there are two kinds of absorption peaks:

- narrow ones labelled A_1, A_2, A_3, which are more easily observed in the diluted crystal (figure 2(a));

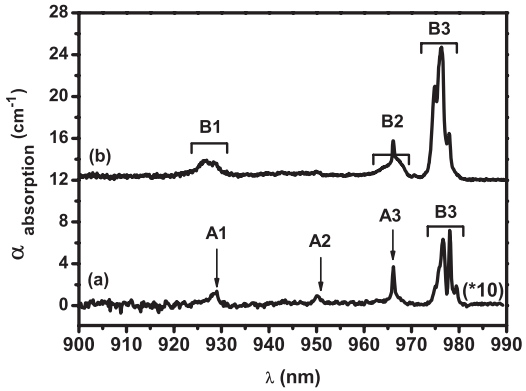

Figure 2. Absorption spectra of $PbF_2 + 0.2\%$ Yb (a) and $PbF_2 + 2\%$ Yb (b) single crystals, recorded at 10 K. The $PbF_2 + 2\%$ Yb spectrum has been translated vertically and the $PbF_2 + 0.2\%$ Yb absorption spectrum has been multiplied by a factor of 10.

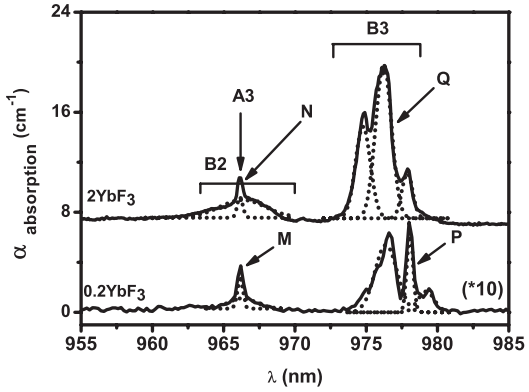

Figure 3. 10 K absorption spectra of $PbF_2 + 0.2\%$ YbF_3 and $PbF_2 + 2\%$ YbF_3. The dotted lines represent the Gaussian fits.

- broad bands B_1 and B_2 (almost superimposed on the narrow lines A_1 and A_3 respectively) and B_3 (composed of several lines), which are particularly strong in the most concentrated sample (figure 2(b)).

To be more specific, figure 3 represents a zoom of the absorption spectra between 955 and 985 nm, on which the absorption bands were fitted with Gaussian lines. Let us call M and P the area of respectively the A_3 and entire B_3 absorption bands of the β-$PbF_2 + 0.2\%$ Yb single crystal and N and Q the corresponding areas for the β-$PbF_2 + 2\%$ Yb single crystal. Assuming that the integrated absorption coefficient is proportional to the concentration of the absorbing species, the ratios $\frac{N}{M}$ and $\frac{Q}{P}$ represent respectively the evolution of the population of the A and B sites when going from $PbF_2 + 2\%$ Yb to $PbF_2 + 0.2\%$ Yb. Without any site preference, they should be equal to 10, but experimentally, $\frac{N}{M} = 5 \pm 0.4$ and $\frac{Q}{P} = 18 \pm 1$. This clearly indicates that the A and B lines belong to different Yb^{3+} species.

The two ratios (5 ± 0.4 and 18 ± 1) for the A and B species respectively must be compared to the ratio (3 ± 1) of the cubic sites found by EPR. The much better agreement between the cubic and the A species ratios strongly suggests to assign the A lines of the absorption spectra to the cubic site of the β-PbF_2 lattice. Luminescence spectroscopy under selective excitation, presented below, will confirm this assumption.

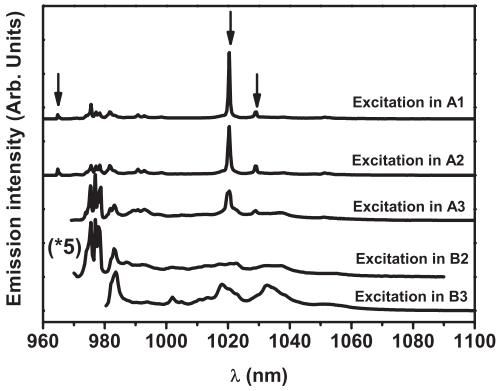

Figure 4. Fluorescence spectra of the $PbF_2 + 0.2\%$ YbF_3 single crystal, under selective excitation, recorded at 10 K. The fluorescence lines corresponding to the A site are indicated by arrows.

The proportion of both types of Yb^{3+} can be evaluated in the two ytterbium-doped β-PbF_2 single crystals using the two additional expressions $N + Q = 2.0\%$ and $M + P = 0.2\%$. The resolution of these equations indicates that, in the β-$PbF_2 + 0.2\%$ Yb single crystal, 61% of the incorporated Yb^{3+} ions occupy cubic symmetry sites, while 39% of the Yb^{3+} are of the B type. In the β-$PbF_2 + 2\%$ Yb single crystal, most of the incorporated Yb^{3+} ions are of the B type and only 31% lie in the cubic sites. The B sites are strongly favoured at high Yb concentration.

The emission spectra of the $PbF_2 + 0.2\%$ Yb single crystal recorded under a selective laser excitation are presented in figure 4. The spectra resulting from excitation in A_1, A_2 and A_3 peaks present very similar lines, with in particular three narrow peaks at 966.6, 1020.3 and 1029 nm, whereas the emission spectra resulting from excitation in the B_1 and B_2 bands present different lines. This confirms the attribution of the absorption bands to the two types of Yb^{3+} and evidences the emission bands corresponding to them.

However, one can notice that, on the emission spectra of the cubic A species, the broad emission situated around 978 nm and belonging to B-type Yb^{3+} is particularly intense under a 966.6 nm excitation. The superimposition of the A_3 peak and the broad B_2 band can explain this phenomenon. Indeed, a 966.6 nm wavelength leads to the excitation of Yb^{3+} of both types at the same time. Consequently, the emission spectrum results in the superimposition of the contributions of the two Yb types A and B. Moreover, an energy transfer from the A to the B Yb^{3+} sites can occur. Such energy transfer is possible, even at 10 K, as there is a good matching between the energy levels of the two types of Yb^{3+} ions.

To conclude, the site-selective laser excitation confirms the presence of two types of Yb^{3+} in β-PbF_2 single crystals. A-type Yb^{3+} occupying cubic symmetry sites (O_h) are observed by EPR and present thin absorption and emission peaks. They will be studied in the following section (section 3.3.2). The second type of Yb^{3+}, labelled type B, is not detected by EPR and presents broad optical bands. Its origin will be investigated in section 3.3.3.

3.3.2. Study of A-type Yb^{3+} ions.

3.3.2.1. Energy level diagram. According to group theory, Yb^{3+} in cubic symmetry site in fluorite-type crystals has its ground multiplet $^2F_{7/2}$ split into three Stark levels, labelled Γ_6, Γ_7 and Γ_8, and its excited level $^2F_{5/2}$ split into two Stark levels, Γ_7' and Γ_8', Γ_7 and Γ_6 being Kramers doublets and Γ_8 a quartet. The g-factor value, determined by EPR in section 1,

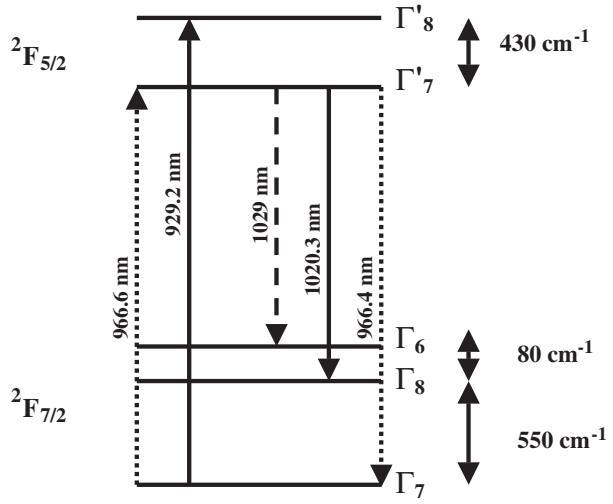

Figure 5. Energy level diagram of Yb^{3+}:β-PbF_2, in cubic symmetry sites (A). Solid lines correspond to ED–MD transitions, dotted lines to MD transitions and dashed lines to ED transitions.

characterizes a Γ_7 ground state [10] as for Yb^{3+} in the cubic sites of the other fluorite-type crystals (table 1). A theoretical crystal-field calculation published in the literature [16] has given the symmetry and order of the other levels.

In the previous section, three absorption bands A_1, A_2 and A_3 have been attributed to cubic Yb^{3+} ions. At $T = 10$ K, only the Γ_7 doublet of the $^2F_{7/2}$ ground multiplet is populated. Therefore, two absorption bands are expected for Yb^{3+} of type A. As the splitting between the two Stark levels of the excited level is usually around 400 cm^{-1} [14], we deduced that the pure electronic transitions correspond to the A_1 (10 764 cm^{-1}) and A_3 (10 346 cm^{-1}) peaks, whereas the absorption peak A_2 results from a vibronic transition. The energy level diagram corresponding to Yb^{3+} in cubic symmetry is represented in figure 5, which also includes the observed transitions and their electric/magnetic dipolar (ED/MD) character. ED transitions are forbidden in cubic (centro-symmetric) symmetry, explaining the very weak intensity of the emission peak at 1029 nm, while MD are allowed since $\Delta J = \pm 1$. Our assignments are in good agreement with those published by Gerasimov *et al* [16].

3.3.2.2. Vibronic transitions. Since the 1020.3 nm emission band is the strongest one, the corresponding fluorescence excitation spectrum of the PbF_2 + 0.2% Yb single crystal was performed at 10 K and is presented in figure 6(a). It exhibits the absorption bands A_1 and A_3, corresponding to the pure electronic transitions, and several other bands, corresponding to vibronic transitions, among which the A_2 band, already detected in the absorption spectrum (table 2), is the strongest one.

The phonon frequencies, associated with Yb^{3+} ions in the cubic site in β-PbF_2, were determined from the vibronic transition observed on the excitation spectrum (figure 6) and are gathered in table 3. According to the phonon spectrum given in the literature [24–26], some vibrations correspond to β-PbF_2 eigenmodes. The other phonon frequencies at 54, 78, 170 and 284 cm^{-1} may correspond to eigen vibration modes of Yb-containing polyhedra. These

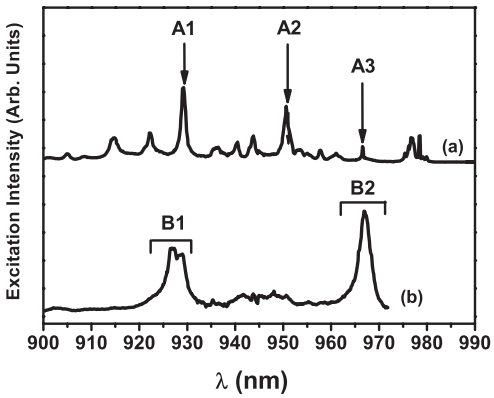

Figure 6. 10 K excitation spectra of $PbF_2 + 0.2\%$ Yb single crystal for (a) the 1020.3 nm emission and (b) the 975 nm emission.

Table 3. Phonon frequencies associated with cubic Yb^{3+} (A) in $PbF_2 + 0.2\%$ Yb single crystal determined using the excitation spectra given in figure 6.

Position (nm)	Pure electronic transition	Experimental phonon frequency (cm^{-1})	Phonon frequency in β-PbF_2 (cm^{-1}) [24, 25]
961.1	$\Gamma_7 \rightarrow \Gamma_7'$	54	—
957.7	(966.6 nm)	92	105
950.6		170	—
943.9		244	250[a]
940.9		284	—
936.1		333	333
922.3	$\Gamma_7 \rightarrow \Gamma_8'$	78	—
914.6	(929 nm)	170	—
908.7		242	250[a]
905.0		285	—
901.1		334	333

[a] The 250 cm^{-1} phonon is the T_{2g} Raman-active mode [26].

phonon energies are in rather good agreement with those reported by Gerasimov: 55, 77, 175, 267 and 342 cm^{-1} [16]. One can notice that the electron–phonon coupling associated with the 170 cm^{-1} phonon is very efficient because it enables us to observe the strongest vibronic transition, associated with the $\Gamma_7 \rightarrow \Gamma_7'$ transition (labelled A_2 in figure 1), on the absorption and excitation spectrum of $PbF_2 + 0.2\%$ Yb.

3.3.2.3. Cooperative fluorescence spectrum. The cooperative fluorescence occurs when two excited ions interact and simultaneously de-excite, emitting one photon whose energy corresponds to the sum of the two excitation energies [27]. Yb^{3+} ions are particularly convenient for observing this emission (situated around 500 nm) as they only have one excited level ($^2F_{5/2}$). The electrostatic interaction is much stronger (at least 100 times) than the magnetic one, which can be neglected [28]. Assuming multipolar interactions between Yb^{3+} ions (such as dipole–dipole or quadrupole–dipole), the cooperative emission probability mainly depends on the distance d between interacting ions [29] and on the transition probabilities for high symmetry centres [30].

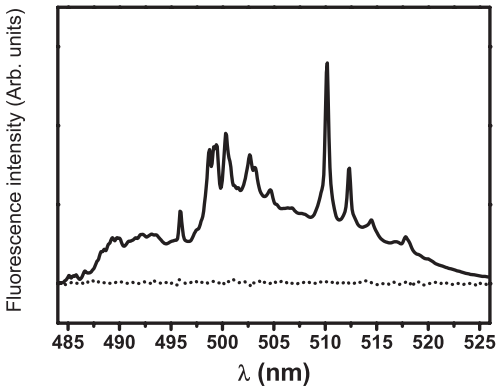

Figure 7. Predicted (solid line) and experimental (dotted line) cooperative fluorescence spectra of cubic Yb^{3+} in $PbF_2 + 0.2\%$ Yb single crystal at $T = 10$ K, under a 950.6 nm excitation.

The cooperative emission was studied in the $PbF_2 + 0.2\%$ Yb single crystal. The more concentrated $PbF_2 + 2\%$ Yb single crystal could not be used because selective excitation of the cubic Yb^{3+} ions was very difficult to achieve. The Yb^{3+} theoretical cooperative emission spectra $F(E)$, resulting from the convolution of the IR emission spectra of Yb^{3+} $f(E)$ by itself, can be calculated by the expression $F(E) = \int f(E')f(E - E')\mathrm{d}E'$ [31].

The predicted spectrum was obtained using the infrared emission spectra recorded under an excitation in A_2 (figure 4), where absorption of the B-type Yb^{3+} is negligible, and is reported in a solid line in figure 7. The convolution predicts in particular an intense peak at 510.2 nm, whose energy corresponds to the sum of two 1020.3 nm photons (strongest fluorescence line). The experimental fluorescence around 500 nm was recorded under a strong excitation at 950.6 nm and using an appropriate detection. It is represented in figure 7 in a dotted line. Clearly, no cooperative emission is observed. Two factors can explain this observation:

- The large distance between Yb^{3+} ions. Indeed, to keep the O_h symmetry, two neighbouring Yb^{3+} ions should be far away from at least a unit cell, i.e. 5.94 Å, preventing efficient cooperative emission.
- The selection rules. It has been pointed out [30] that no cooperative emission can be observed for identical Yb^{3+} ions occupying centrosymmetric positions (this is the case for Yb^{3+} in the O_h symmetry site), forbidding the electric dipole transitions. Magnetic dipole interactions are too weak to be observed.

3.3.3. Study of the B-type Yb^{3+}. The main absorption band B_3 attributed to Yb^{3+} of type B is very intense and dominates the absorption spectrum of PbF_2 doped with 0.2% or 2% Yb. A broad and strong absorption band similar to B_3 has already been observed by Abbruscato *et al* in 0.15% YbF_3 doped CdF_2 [15]. The authors proposed to assign it to the formation of exchange coupled pairs of Yb^{3+}. Moreover, the B_3 band has already been observed in YbF_3-doped β-PbF_2 crystals [16], but its origin has not yet been determined.

3.3.3.1. Energy level diagram. Using the absorption (figure 2) and emission (figure 4) spectra previously discussed, the energy level diagram of the second site of Yb^{3+} was drawn and is presented in figure 8. It shows that the $^2F_{5/2}$ level splits into three Stark levels, indicating a complete lifting of the degeneracy into Kramers doublets. This shows that the symmetry of the B sites is lower than cubic. Only three of the four Kramers levels expected for the $^2F_{7/2}$

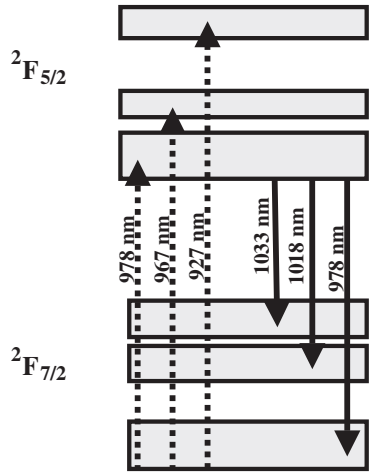

Figure 8. Energy level diagram of the B type (clusters) of Yb^{3+} ions. The level thickness reflects the important line-width of the absorption and emission bands.

ground state of the B sites are experimentally found (figure 8). It is likely that two of these levels are close to each other, compared to the individual linewidth, and cannot be separated on the fluorescence spectra.

One can observe that the absorption and emission bands are much broader than those of the Yb^{3+} of type A. This could reveal an inhomogeneous broadening that has been reflected in figure 8 by a thickness of the energy levels. However, one can notice that the B_3 band is made of at least three or four major components in both single crystals (figure 3). The relative intensities of these components vary with the Yb concentration (figure 3), indicating some preferential site occupancy, and the emission spectra resulting from excitation at different wavelengths in the B_3 band are slightly different. One can conclude that not all the B sites occupied by Yb^{3+} ions are strictly equivalent, but that there are at least three different sub-types, explaining the resolution into several components and the broadening of the optical transitions.

The 975 nm excitation spectrum of $PbF_2 + 0.2\%$ Yb is reported in figure 6(b). Except the strong absorption bands B_1 and B_2, corresponding to purely electronic transitions, a continuous background was observed all over the spectra, indicating that a large number of vibronic lines also occurs for the Yb^{3+} B type. However, individual phonon frequencies were impossible to determine.

3.3.3.2. Cooperative emission. The cooperative emission of $PbF_2 + 0.2\%$ Yb was recorded at $T = 10$ K under a 968.6 nm excitation whose ordinary fluorescence is reported in figure 4. Both calculated and experimental spectra are represented in figure 9, respectively in solid and dotted lines. There is a good correlation between the two spectra. Whereas no cooperative emission was observed when exciting Yb^{3+} ions in a cubic symmetry site, B-type Yb^{3+} ions give strong cooperative emission.

3.3.3.3. Assignment of the Yb^{3+} B type. In MF_2 single crystals, it was been widely demonstrated that Yb^{3+} ions formed dimers and clusters [32–34], even at low concentration (>0.01% [35]), which have for instance been identified using optically detected EPR [36]. In lanthanide ion (Ln) doped fluorite single crystals, several cluster models have been proposed mainly based on EXAFS and neutron scattering studies [37]. The most reliable model is an

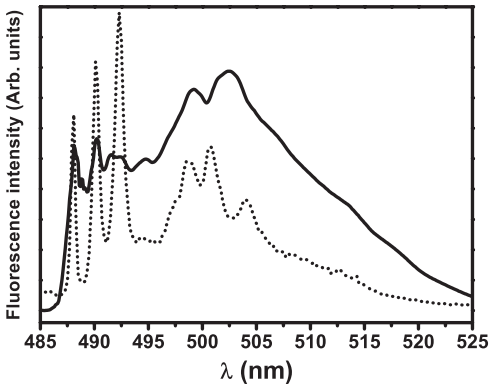

Figure 9. Calculated (solid line) and experimental (dotted line) cooperative emission spectra of the Yb^{3+} clusters in $PbF_2 + 0.2$ Yb single crystal at $T = 10$ K. Excitation wavelength: 968.6 nm.

Ln_6F_{37} cluster [38], made of Ln ions, regular and interstitial F^- ions and vacancies, in which the Ln site symmetry is roughly tetragonal [38]. These clusters can be easily incorporated into the MF_2 lattice because its structure and shape are identical to the M_6F_{32} unit of the fluorite lattice.

The above results suggest assigning the B site to Yb^{3+} forming 'hexameric' clusters inside the β-PbF_2 lattice. Indeed, as shown above, the B Yb^{3+} ions are strongly favoured at high doping rate, as expected for clusters. According to the structural information available on these clusters [39], the Ln site symmetry is roughly tetragonal, which agrees with the energy level diagram discussed above. Furthermore, with such a complicated structure, it is likely that small departure from axial symmetry occurs from one Yb^{3+} ion to another in the cluster [39], explaining the complex structure of the B_3 band for instance and, more generally, the broadness of the B bands. At last, the strong cooperative fluorescence observed for the B Yb^{3+} ions implies that the Yb^{3+} ions giving rise to this cooperative emission are close to each other. Indeed, in these clusters, Yb–Yb distances are about 3 Å [40], to be compared with the cubic site distance of ∼6 Å that does not give rise to cooperative fluorescence (figure 7).

3.3.3.4. Correlation with EPR signal. As seen before (section 3.2), the standard EPR spectrum of $PbF_2 + 0.2\%$ Yb and $PbF_2 + 2\%$ Yb single crystals only shows Yb^{3+} ions in cubic symmetry site. However, Yb^{3+} ions forming clusters have been detected using optically detected EPR [36, 41] in the system CaF_2:Yb. In such clusters, it has been demonstrated by crystal field calculations [38] that the strong tetragonal crystal field leads to a ground state which is a pure $M_J = \pm 7/2$ Kramers doublet. The magnetic field lifts the degeneracy of the two components of the ground state, but $|\Delta M_J| = 7$, instead of the value 1 required by the magnetic dipolar selection rule applying to the standard EPR technique used here. Therefore, the EPR transitions of the B-type Yb^{3+} ions forming clusters are forbidden and undetectable.

3.3.4. Comparison of the A and B optical properties. It must be pointed out that the optical properties of Yb-doped PbF_2 crystals are primarily due to the Yb^{3+} clusters, even if the cubic site is the most populated, as in the β-$PbF_2 + 0.2\%$ Yb single crystal. Knowing the proportion of A- and B-type Yb^{3+}, it is possible to calculate the absorption cross-section σ of each species from the absorption spectra given in figure 3. One obtains $\sigma_{A_3} = 1.4 \times 10^{-20}$ cm^2 for the strongest absorption line of the cubic site and $\sigma_{B_3} = 10.0 \times 10^{-20}$ cm^2 for the dominant

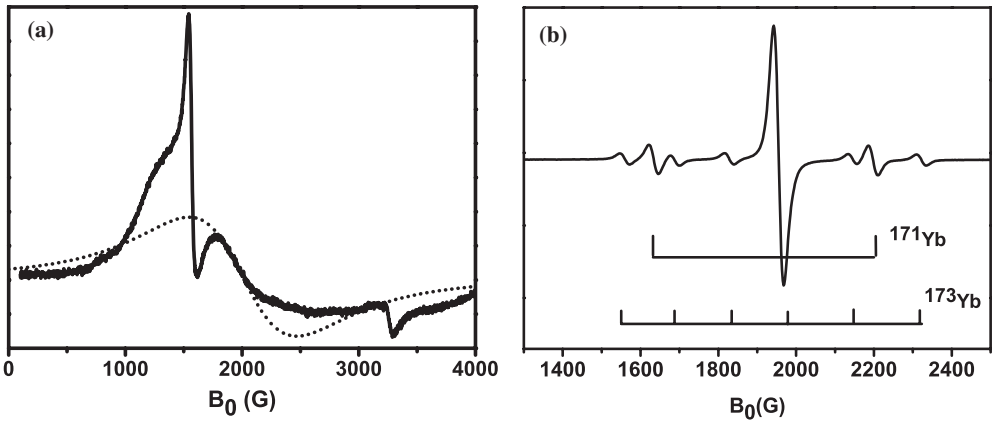

Figure 10. EPR spectrum of (a) P22Y005 glass and (b) the corresponding glass-ceramic. $T = 10$ K; $\nu = 9.40$ GHz.

absorption component of the B_3 band of the Yb^{3+}-forming clusters. In calculating this cross-section, we have assumed that the number of Yb^{3+} ions absorbing at the peak wavelength is proportional to the area of the component with respect to the entire B_3 band. The difference between the A and B cross-sections comes primarily from the centro-symmetric character of the cubic sites, which forbids ED optical transitions. The observed absorption is of pure MD character and therefore σ_{A_3} is very small. In contrast, the absorption cross-section of the clusters is large because the site symmetry is at most tetragonal and the ED transitions are allowed. Moreover, it has been recognized in other systems containing transition metal ions that magnetic interactions can enhance the optical transition probabilities [42]. Here, we are dealing with lanthanide ions, which generally undergo weaker magnetic interaction than transition metal ions. Nevertheless, a role of such interactions to increase the absorption of the clusters cannot be excluded. It is likely that Yb^{3+} clusters are also responsible for the interesting laser properties, as observed in other ytterbium activated fluorite materials, such as Yb^{3+}:CaF_2 single crystals for instance [43, 44].

4. Investigation of the parent glasses: results and discussion

4.1. EPR spectra of glasses

The EPR spectra of P22Y005 and P10Y3 glasses were recorded at $T = 10$ K, a temperature suitable to observe the Yb^{3+} signal. The P22Y005 glass spectrum is shown in figure 10(a) in a solid line. It is composed of a broad spectral line, lying between 0 and 4000 G, and of narrow peaks superimposed on it. These narrow peaks, still visible above 100 K, correspond to the perpendicular and parallel components of an EPR spectrum attributable to the paramagnetic ion Fe^{3+} ($g_\parallel = 2.03$ and $g_\perp = 4.28$), as reported in the literature [45]. These iron ions have been introduced as impurities in the compounds (probably in GeO_2) used in the glass synthesis.

The broad line intensity decreases and broadens without deformation when the temperature increases. Finally, it completely disappears at $T = 50$ K, indicating that the paramagnetic species responsible for this line has a very fast relaxation time, typically Yb^{3+} ions. The absence of line deformation proves that there is only one type of Yb^{3+} ions in the glass. If different Yb^{3+} species were occurring in the glass, it is likely that they would have different relaxation times T_1 and consequently different behaviours upon warming the glass.

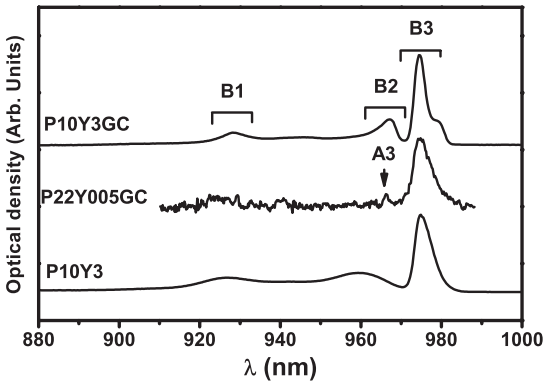

Figure 11. $T = 10$ K absorption spectra of P10Y3 glass, P22Y005GC and P10Y3GC glass-ceramics.

The Yb^{3+} signal, obtained by subtracting the Fe^{3+} signal, is represented in a dotted line in figure 10(a). The spectral line is centred at $g = 3.34 \pm 0.05$, with a linewidth of 920 G. This linewidth corresponds to the inhomogeneous broadening of one mean type of Yb^{3+} ions distributed in various environments. According to the symmetry of the line and its g value, close to the one of cubic Yb^{3+} in PbF_2 single crystals ($g_{cub} = 3.435$, see section 3.2), it may be proposed that, even in the glass, the Yb^{3+} environment is close to cubic symmetry and similar to the one found in β-PbF_2 crystals. The absence of parallel and perpendicular components characteristic of the EPR powder spectrum, in the case of axial symmetry for instance, reinforces the assumption of average cubic symmetry for Yb^{3+} in the glass.

The EPR spectrum of P10Y3 glass is similar to the one of P22F005 glass but broader (peak-to-peak linewidth of 1150 G instead of 920 G). As the glass contains much more Yb, the Yb^{3+} signal is more intense and hides the Fe^{3+} signal.

4.2. Optical absorption of glasses

The absorption spectrum of P10Y3 glass was recorded at 10 K and is reported in figure 11. The observed absorption peaks are similar to the B bands found in the PbF_2 single crystals (figure 2), in spite of an inhomogeneous broadening, as usual in glasses. This indicates the presence in the glass of Yb^{3+} in an environment close to the one of B-type Yb^{3+}, i.e. Yb^{3+} forming clusters.

The absorption lines of Yb^{3+} in a environment close to cubic symmetry and detected by EPR are not visible on the glass spectrum for two reasons: first, the absorption cross-sections of these Yb^{3+} ions may be smaller than the ones of B-type Yb^{3+} and second the concentration of Yb^{3+} (3%) in the glass favours the formation of B-type Yb^{3+}.

The EPR and optical observations evidence the presence of two types of Yb^{3+} in the glass: Yb^{3+} in an environment close to the cubic symmetry found in the PbF_2 single crystals and Yb^{3+} close to the B type, previously described (see section 3.3.3). This reveals that, in the glass, Yb^{3+} is already in fluoride environments close to those found in the single crystals and in the glass-ceramics (see section 5).

This conclusion can also be correlated to the comparison of the nucleating efficiency of erbium-containing compounds (ErF_3, ErOF and Er_2O_3), previously studied in these GeO_2:PbO:PbF_2 glasses [46]. Indeed, it has been demonstrated that only ErF_3 was a nucleating agent for the heterogeneous nucleation of PbF_2. It has been postulated that there was a memory

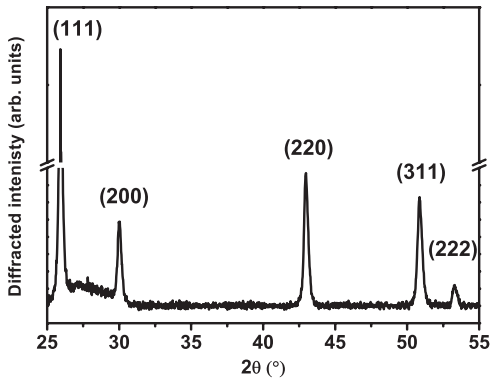

Figure 12. XRD diagram ($\lambda_{Cu} = 1.5406$ Å) of P22Y005GC glass-ceramic.

Table 4. Unit cell parameter a of β-PbF_2 single crystals and glass-ceramics.

Sample	Ratio YbF_3/PbF_2	Unit cell parameter a (Å)
Pure β-PbF_2 single crystal	0%	5.94 (see footnote 2)
Single-crystal $PbF_2 + 0.2\%$ YbF_3	0.2%	5.930 ± 0.005
Single-crystal $PbF_2 + 2\%$ YbF_3	2%	5.905 ± 0.005
P22Y005GC glass-ceramic	0.23%	5.920 ± 0.005
P10Y3GC glass-ceramic	30%	5.780 ± 0.005

effect and that Er^{3+} ions kept their fluoride environment in the glass. This was confirmed through the study of Er^{3+} lifetime [47].

The similarities of the environment of Er^{3+} in the glass and in the corresponding glass-ceramic were also mentioned in a different system, with the composition SiO_2:Al_2O_3:CdF_2:PbF_1:ZnF_2:ErF_3 [8].

5. Investigation of the transparent Yb-doped glass-ceramics: results and discussion

5.1. X-ray diffraction

The XRD diagrams of the glass-ceramics P10Y3GC and P22Y005GC were performed and one of them is presented on figure 12. It is composed of the diffraction peaks of the β-PbF_2 cubic phase superimposed on the diffuse scattering of the remaining amorphous oxide phase in the 2θ range 25°–32°, highlighting the biphasic structure of the glass-ceramic. Using the Scherrer formula, the size of the PbF_2 crystallites was calculated to be 26 ± 1 nm in P22Y005GC and 13 ± 1 nm in P10Y3GC. As demonstrated in [5], YbF_3 is a nucleating agent for the PbF_2 phase. Consequently, the higher the ratio $\frac{YbF_3}{PbF_2}$, the smaller the crystallites.

The values of the unit cell parameter of the ytterbium doped lead fluoride crystallites are gathered in table 4, with those of the single crystals. One can observe that a strong decrease of the unit cell parameter is also observed in the glass-ceramics when the ratio $\frac{YbF_3}{PbF_2}$ increases from 0 to 30%. As for β-PbF_2 single crystals (see section 3.1), the decrease of the unit cell parameter indicates the substitution of Pb^{2+} by Yb^{3+}. Hence, Yb^{3+} ions are incorporated into the crystallites during the glass devitrification, forming a β-$Pb_{1-y}Yb_yF_{2+y}$ solid solution.

The comparison between the crystallite and single-crystal composition reveals that the unit cell parameter a of the crystallites of P22Y005GC glass-ceramic is slightly larger than the one

of $PbF_2 + 0.2\%$ Yb single crystal, with respect to the measurement uncertainty. It proves that Yb concentration inside the crystallites of P22Y005GC is slightly above 0.2%. As the ratio $\frac{YbF_3}{PbF_2}$ is 0.23, it reflects the complete segregation of Yb^{3+} ions inside the crystallites of P22Y005GC glass-ceramics. This phenomenon can be compared to the segregation of Er^{3+} ions recently demonstrated in Er^{3+}-doped glass-ceramics [18]. Similarly, in the P10Y3GC glass-ceramic, the complete segregation of Yb^{3+} into the crystallites leads to a local Yb concentration of 30%.

5.2. EPR spectra of the glass-ceramics

The EPR spectrum of the P22Y005GC glass-ceramic was also recorded at 10 K and is represented on figure 10(b). One can notice that the broad band characterizing Yb^{3+} ions in glasses has disappeared, evidencing the change of environment of Yb^{3+} ions during the devitrification process. The glass-ceramic EPR linewidth (26 G) is much narrower than in the glass (920 G), demonstrating that Yb^{3+} ions are incorporated into a well defined crystalline environment. EPR also evidences the segregation of Yb^{3+} inside the crystallites and is in really good agreement with the conclusions of the XRD study (see section 5.1).

Although the glass-ceramic is made of many crystallites randomly oriented in the glassy matrix, its EPR spectrum is composed of one intense central line, surrounded by the hyperfine satellites, and is identical to those of Yb^{3+} in β-PbF_2 single crystals. This observation reveals that Yb^{3+} has a cubic symmetry (O_h) in the PbF_2 crystallites of the glass-ceramics, as in β-PbF_2 single crystals.

The EPR spectrum of P10Y3GC glass-ceramic was also recorded at 10 K. However, the spectrum exhibits only a broad band (line-width ~900 G) centred at $g = 3.34$ and no hyperfine satellites are visible. The broadness of the spectrum reflects the presence of very strong Yb–Yb dipolar interactions [23], indicating a high Yb^{3+} local concentration in the crystallites and consequently a high Yb segregation into the crystallites. This is again in agreement with the result deduced from the measurement of the unit cell parameter (see section 5.1).

5.2.1. Optical spectra of the glass-ceramics. The absorption spectra of P22Y005GC and P10Y3GC glass-ceramics, recorded at low temperature, are presented of figure 11. The absorption spectrum of P22Y005GC glass-ceramic exhibits a broad band at 978 nm, similar to the B_3 band of the single crystals, proving the presence of Yb^{3+} clusters in the nanocrystallites of the glass-ceramic. At 966.6 nm (A_3 line), a small and narrow peak, pointed with an arrow in figure 11, is observed. This indicates the presence of Yb^{3+} ions in cubic symmetry sites, in agreement with the EPR results. The rest of the spectrum is difficult to analyse, due to the low signal/noise ratio. Indeed, the global Yb concentration in this sample is quite low (0.05%), preventing the recording of a better-resolved absorption spectrum. One can conclude that, as in the Yb-doped PbF_2 single crystals, there are two types of Yb^{3+} ions, cubic ones and clusters, in the P22Y005GC glass-ceramic.

The absorption spectrum of the P10Y3GC glass-ceramic (figure 11) presents a broad and intense band, centred at 978 nm, followed by two broad bands at 967 and 927 nm. These absorption bands are identical to the B_3, B_2 and B_1 bands of the single crystals previously studied. According to the optical study, in the P10Y3GC glass-ceramic Yb^{3+} ions exclusively form clusters. As observed for the single crystals, this is due to the high Yb concentration.

6. Conclusion

In the glass-ceramics, as well as in the Yb^{3+}-doped β-PbF_2 single crystals, there are two types of Yb^{3+} ions: A type, corresponding to Yb^{3+} in cubic symmetry sites, and B type, forming

clusters. The relative proportion of the two species varies according to the Yb concentration. Yb^{3+} in cubic sites is the major species at very low concentration, while Yb^{3+} clusters dominate at higher doping levels. The optical transitions of the Yb^{3+} clusters are much stronger than the cubic Yb^{3+} ones, thanks to the lack of inversion centre. They may be responsible for the interesting optical properties evidenced in other Yb^{3+} activated fluorite crystals, like CaF_2 for instance.

In the transparent oxyfluoride glass-ceramics, containing β-$Pb_{1-y}Yb_yF_{2+y}$ nanocrystallites, XRD and EPR evidenced the complete segregation of Yb^{3+} ions into the β-PbF_2 crystallites during the devitrification process. The optical properties of the glass-ceramics look very similar to those of the Yb^{3+}-doped single crystals. Therefore, they are potentially interesting for laser applications, either in bulk or fibre form. Investigation of the possibility to fabricate optical fibres and studies of the laser properties of these materials are in progress.

References

[1] Kennedy J H, Miles R and Hunter J 1973 *J. Electrochem. Soc.* **120** 1441–6
[2] Mho S and Wright J C 1983 *J. Chem. Phys.* **79** 3962–75
[3] Mortier M 2002 *Phil. Mag.* B **82** 745–53
[4] Wang Y and Ohwaki J 1993 *Appl. Phys. Lett.* **63** 3268–70
[5] Dantelle G, Mortier M, Vivien D and Patriarche G 2005 *J. Mater. Res.* **20** 472–81
[6] Samson B N, Tick P A and Borrelli N F 2001 *Opt. Lett.* **26** 145–7
[7] Kulakov A B, Zhokhov A A, Emel'chenko G A and Klassen N V 1995 *J. Cryst. Growth* **151** 107–13
[8] Tikhomirov V K, Furniss D, Seddon A B, Reaney I M, Beggiora M, Ferrari M, Montagna M and Rolli R 2002 *Appl. Phys. Lett.* **81** 1937
[9] Cheetham A K, Fender B E F and Cooper M J 1971 *J. Phys. C: Solid State Phys.* **4** 3107
[10] Weber M J and Bierig R W 1964 *Phys. Rev.* A **134** A1492–503
[11] Eicken J, Gunsser W, Chernov S V, Glumov A V and Murien I V 1992 *Solid State Ion.* **55/56** 843
[12] Patwe S J, Balaya P, Goyal P S and Tyagi A K 2001 *Mater. Res. Bull.* **36** 1743
[13] Kirton J and McLaughlan S D 1967 *Phys. Rev.* **155** 279–84
[14] Falin M L, Gerasimov K I, Latypov V A and Leushin A M 2003 *J. Phys.: Condens. Matter* **15** 2833–47
[15] Abbruscato V J, Banks E and McGarvey B R 1968 *J. Chem. Phys.* **49** 903–11
[16] Gerasimov K I, Leushin A M and Falin M L 2001 *Phys. Solid State* **43** 1675–9
[17] Rodriguez V D, Tikhomirov V K, Mendez-Ramos J and Seddon A B 2005 *Europhys. Lett.* **69** 128
[18] Dantelle G, Mortier M, Patriarche G and Vivien D 2006 *J. Solid State Chem.* **179** 1995
[19] Mortier M and Patriarche G 2000 *J. Mater. Sci.* **35** 4849–56
[20] Samara G A 1976 *Phys. Rev.* B **13** 4529–44
[21] Tyagi A K, Patwe S I, Achary S N and Mallia M B 2004 *J. Solid State Chem.* **177** 1746–57
[22] Sherstkov Y A, Azarov V V, Rybakov V A and Gorlov A D 1975 *Sov. Phys.—Solid State* **17** 384–5
[23] Pake G E and Estle T L 1973 *The Physical Principles of Electron Paramagnetic Resonance* 2nd edn (Reading, MA: Benjamin)
[24] Dickens M H and Hutchings M T 1978 *J. Phys. C: Solid State Phys.* **11** 461–8
[25] Sahni V C and Jacobs P W M 1983 *J. Phys. C: Solid State Phys.* **16** L241–5
[26] Kessler J R, Monberg E and Nicol M 1974 *J. Chem. Phys.* **60** 5057–65
[27] Nakazawa E and Shionoya S 1970 *Phys. Rev. Lett.* **25** 1710–2
[28] Goldner Ph, Pelle F and Auzel F 1997 *J. Lumin.* **72–74** 901–3
[29] Goldner Ph, Schaudel B and Prassas M 2002 *Phys. Rev.* B **65** 054103
[30] Ovsyankin V V, Podkolzina I G and Fedorov A A 1979 *Izv. Akad. Nauk SSSR Ser. Fiz.* **43** 1194–202
[31] Kushida T 1973 *J. Phys. Soc. Japan* **34** 1318–26
[32] Laval J P, Abaouz A and Frit B 1989 *J. Solid State Chem.* **81** 271–7
[33] Kurz M D and Wright J C 1977 *J. Lumin.* **15** 169–86
[34] Bendall P J, Catlow C R A, Corish J and Jacobs P W M 1984 *J. Solid State Chem.* **51** 159–69
[35] Fenn K B, Wright J C and Fong F K 1973 *J. Chem. Phys.* **59** 5591–9
[36] Kazanskii S A 1985 *Sov. Phys.—JETP* **62** 727–33
[37] Laval J P, Abaouz A, Frit B and Le Bail A 1990 *J. Solid State Chem.* **85** 133–43

[38] Nikiforov A E, Zakharov A Y, Ugryumov M Y, Kazanskii S A, Ryskin A I and Shakurov G S 2005 *Phys. Solid State* **47** 1431–5
[39] Kazanskii S A, Ryskin A I, Nikiforov A E, Zaharov A Y, Ougrumov M Y and Shakurov G S 2005 *Phys. Rev.* B **72** 014127
[40] Tyagi A K and Köhler J 2001 *Solid State Sci.* **3** 689–95
[41] Kazanskii S A and Ryskin A I 2002 *Phys. Solid State* **44** 1415–25
[42] Ferguson J, Guggenheim H J and Tanabe Y 1965 *J. Appl. Phys.* **36** 1046–7
[43] Ito M, Goutaudier C, Guyot Y, Lebbou K, Fukuda T and Boulon G 2004 *J. Phys.: Condens. Matter* **16** 1501–21
[44] Petit V, Doualan J L, Camy P, Ménard V and Moncorgé R 2004 *Appl. Phys.* B **78** 681–4
[45] Tsiskarishvili G and Lundstrom T 1989 *Phys. Chem. Glasses* **30** 160
[46] Mortier M 2003 *J. Non-Cryst. Solids* **318** 56–62
[47] Mortier M, Château C, Genotelle M and Gardant N 2003 *J. Non-Cryst. Solids* **326/327** 287–91